Synthesis and characterization of perovskite $FAPbBr_{3-x}I_x$thin films for solar cells

B. Slimi[a,b,d]●M. Mollar[d]●I. Ben Assaker[a] ●A. Kriaa[c]●R. Chtourou[a]●B. Marí[d]

Received: ……/Accepted …

Abstract: $FAPbI_3$, $FAPbBr_3$ and $FAPbBr_{3-x}I_x$ perovskite thin films were produced in a single step from a solution containing a mixture of FAI, PbI_2, FABr, and $PbBr_2$ (FA=Formamidinium). $FAPbBr_{3-x}I_x$ perovskite thin films were deposited onto ITO-coated glass substrates by spin coating. X-ray diffraction analyses confirmed that these thin film perovskites crystallize in the cubic phase (Pm-3m) for all composition range $0 \leq x \leq 3$. Mixed lead perovskites showed a high absorbance in the UV–vis range. The optical bandgap was estimated from spectral absorbance measurements. It was found that the onset of the absorption edge for $FAPbBr_{3-x}I_x$thin films ranges between 1.47 and 2.20 eV for x=0 and x=3, respectively. Photoluminescence emission energies for mixed halide perovskites were also dependent on their composition and presented intermediate values from 810.4 nm for $FAPbI_3$ to 547.3 nm for $FAPbBr_3$.

Keywords: Organic-inorganic perovskites● Formamidinium Lead Iodide● Formamidinium Lead Bromide● X-Raydiffraction● Optical absorption ● Photoluminescence

✉Bernabé Marí
bmari@fis.upv.es

[a] Laboratoire de Nanomatériaux et Systèmes pour les Energies Renouvelables (LANSER), Centre de Recherches et des Technologies de l'Energie Technopole Borj Cedria, Bp 95, Hammam Lif 2050, Tunisie
[b] Faculté des Sciences de Bizerte, Université de Carthage, Tunisie
[c] Laboratoire de Chimie Moléculaire Organique, 5 Avenue Taha Houssein Monfleury, 1089 Tunis, Tunisie
[d] Departament de Física Aplicada-IDF. Universitat Politècnica de València, Camí de Vera s/n 46022 València, Spain

Introduction

Organometal halide perovskites are currently one of the most actively researched materials. They are typically composed of an organic group (A), a metal ion (B), and one or two halides (X) forming the perovskite structure ABX_3. These hybrid perovskites have become one of the most attractive and promising materials for photovoltaic over the last five years. In particular, the methylammonium (MA) lead halide and formamidinium (FA) lead halide perovskites, namely, $CH_3NH_3PbX_3$ (or $MAPbX_3$) and $CH(NH_2)_2PbX_3$ (or $FAPbX_3$) (X = Br, I, Cl) show remarkable properties for photovoltaic applications [1- 4] and light emitting diodes [5]. Solar power conversion efficiencies of more than 20% have been reported [6], and tunable light emitting diodes have been also reported [7]. Their low cost and ease of production make them potential candidates for future technologies. Due to their great absorption coefficient and high charge carrier mobility, these groups of perovskites are well suited for converting solar energy [8, 9]. In fact, halide perovskites drew an important impact in the field of thin film photovoltaics in the last years, boosting up the energy conversion efficiency from 3.8%,for the first perovskite-based solar cells in 2009 [1], up to more than 20% [6,10-15].

Among these perovskites, $MAPbI_3$is, by far, the most widely studied perovskite for solar cell applications [13-15]. However, the $FAPbI_3$

perovskite with broader light absorption has been attracting increasing interest [6, 10, 16-25]. Like for $MAPbI_3$, typical routes for depositing $FAPbI_3$ perovskite thin films include one-step [6, 18, 21] and sequential deposition methods [6, 16, 19] have been studied. More recently, many studies focusing on material properties directly related to device performance, such as carrier mobilities, recombination lifetimes, excitonic properties and optical absorption have been published [26-29]. Increasing the photocurrent by expanding the absorption spectra of ABX_3 perovskites through chemical modification has been proposed as a method for further improving solar cell efficiency. For example, replacing the MA cation in $MAPbI_3$with a FA cation, which has a larger ionic radius, results in an ABX_3 perovskite with a smaller bandgap for broader-spectrum light harvesting.

$FAPbI_3$, $MAPbI_3$ perovskites as well as their mixed halide analogues ($(FA,MA)Pb(I_{1-x}Br_x)_3$, $(FA,MA)Pb(I_{1-x}Cl_x)_3$) have been already reported [3, 30-33]. In addition, most fractional mixtures of $FAPb(Br_xI_{1-x})_3$ were found to be crystalline, with the exception of the region between $x<0.3$ and $x>0.5$ where the crystal structure changed [19, 34, 35]. By increasing the [Br/I] ratio in the mixed halide perovskite film, it is possible to tune the bandgap from 2.43 to 1.48 eV with a continuous red shift [34].

Such mixed halide films also offer tunability of the emission following bandgap excitation [36]. Such tunable and coherent light emission properties have been utilized in lasing applications [37, 38].

In this paper, we present a study of the crystalline structure, absorption and emission properties of pure ($FAPbI_3$, $FAPbBr_3$) and mixed halide perovskites ($FAPbBr_{3-x}I_x$) synthesized in a single step via drying in DMF solution at a different temperature on ITO substrates as a function of the Br/I ratio.

2. Results and Discussion

2.1. XRD results

Fig. 1a shows the X-ray diffractograms for $FAPbI_3$ powder annealed at140 and 180 °C, respectively. Both powder diffractograms correspond to the same cubic structure corresponding to the spatial group labeled as Pm-3m (a= 6.357 Å). The most intense diffraction peak located below 14° (13.86°) corresponds to (001) diffraction planes and the peaks located at about 20, 24, 28, 31and 40°are related to (1 1 0), (111), (0 0 2), (2 1 0) and (220) diffraction planes, respectively. This corresponds to the α-$FAPbI_3$ phase of our perovskite and not to the δ-$FAPbI_3$ phase characterized by a peak at 11.8° (100). The sharp diffraction peaks indicate the high crystallinity of the as-synthesized $FAPbI_3$ compound. Rietveld refinement analysis of the X-ray powder diffraction pattern reveals that the synthesized

$FAPbI_3$ is a pure phase with the space group of Pm-3m, which was in good agreement with recent reports [3, 29, 30, 39,40].

Fig. 1b shows the X-ray diffractograms for $FAPbI_3$ thin films annealed at 140, 150 and 170 °C in air for 30 min. The same cubic structure corresponding to the spatial group labeled Pm-3m was observed for all samples. The reflection at 2θ=11.8° is correlated to δ-$FAPbI_3$ (yellow phase), while the peak at 2θ≈14° represents the α-$FAPbI_3$ (black phase). As shown, the yellow δ-phase of $FAPbI_3$was produced at annealing temperatures below 150 °C, as indicated by the peak at 11.8°. After annealing at 170 °C the secondary phase, δ-$FAPbI_3$, almost disappears. In this figure, the diffraction peaks corresponding to ITO substrates have been also labelled.

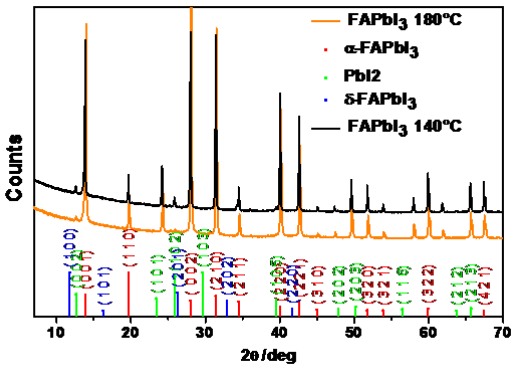

Fig. 1a Typical XRD pattern of the $FAPbI_3$ powder at 140 and 180 °C.

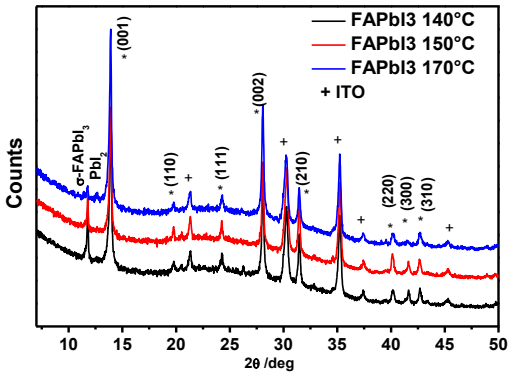

Fig. 1b XRD patterns of $FAPbI_3$ thin films at 140, 150 and 170 °C.

Hybrid perovskite materials in the form of $FAPbBr_{3-x}I_x$ (x= 0-3) were synthesized via spin-coating deposition. Fig. 2 (a, b) shows XRD patterns of $FAPbBr_{3-x}I_x$ prepared with different molar ratios of Br to I at room temperature. In this case, all the films with different iodide contents have

been annealed at 150 °C in air for 30 min. After increasing iodide contents, the XRD measurements show a shift toward low angles for all diffraction planes (labelled as '*' in Figure 2b). This shift is related to an increase in the crystal lattice [19, 27]. The diffraction angle decreases with the increase in iodide contents, in agreement with the bigger size of iodide relative to bromide, which expands the crystal lattice. $FAPbBr_{3-x}I_x$ adopts a cubic structure with a space group of Pm-3m. The gradual shift in the diffraction angle (with the presence of single intense peaks) is a strong indication that a mixed phase of $FAPbBr_{3-x}I_x$is formed in which the two anions are both inserted in the same lattice frame.

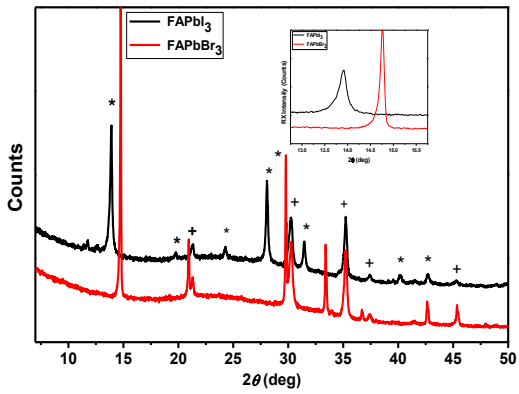

Fig. 2a X-Ray diffractograms of the $FAPbI_3$ and $FAPbBr_3$ thin films.

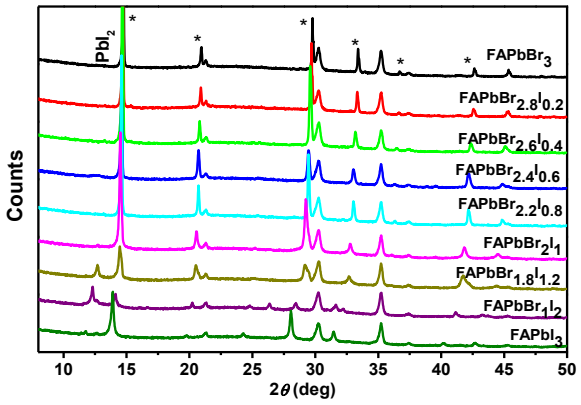

Fig. 2b X-Ray diffractograms of $FAPbBr_{3-x}I_x$ thin film perovskites with Br/I molar ratios from 0 to3.

With the increase of iodide concentration, the position of diffraction peaks shifts to lower angles meaning larger interplanar distances. For all samples, as shown in Fig. 2c, strong peaks are detected at 14° and 28°,

corresponding to the (0 0 1) and (0 0 2) planes, respectively. Such observation confirms the formation of a cubic perovskite structure.

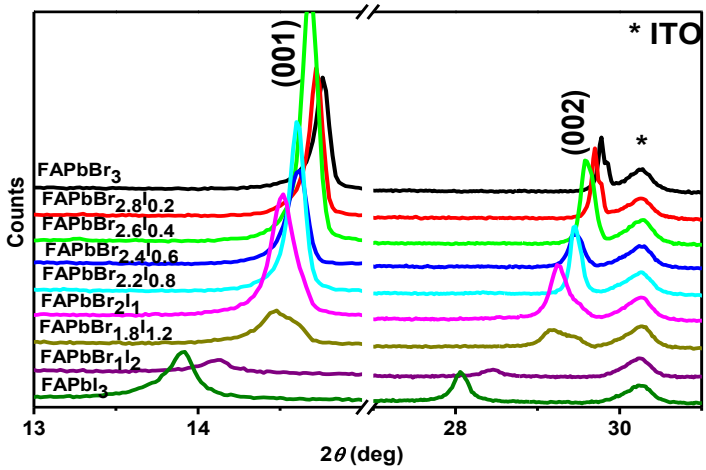

Fig.2c X-Ray diffractograms for $FAPbBr_{3-x}I_x$ thin films. Magnified view of regions 13-16° and 27-30°.

The (001) peak of the α-phase ($2\theta \approx 14°$) consistently shifts to higher angles with higher Br ratio, corresponding to smaller lattice constants. The lattice constants were calculated by fitting the whole pattern using JADE software. For the $FAPbBr_{3-x}I_x$ perovskite, the material is in a single phase throughout the entire composition range. The monotonic shift of the (001) reflection that we observed from $2\theta \approx 14.7°$ to 13.9° (Table 3) is consistent with a shift of the cubic lattice constant from 6.306 to 5.955 Å as the material incorporates a larger fraction of the smaller halide Br [19,27]. It was found that the lattice constant follows the so-called Vegard's law which states that lattice constants vary linearly with the ratio between the two halide components of the thin films [32, 41].

For the pure $FAPbI_3$ film, the intensity of the peak near 12° corresponding to the δ-phase decreases with increasing the annealing temperature from 140 to 170 C°. This phase can disappear totally for an annealing temperature higher than 170 C°. Since perovskites with higher bromide content have a smaller lattice constant than those with higher iodide contents, this splitting is consistent with the presence of a minority phase with significantly enhanced (x>1) iodide contents and a majority phase with slightly enhanced bromide contents (x<1) compared to the original material. If we compare the magnitude of XRD intensity from the two phases, we estimate that the minority phase represents 30% of the material (Fig. 2a), after taking into account, the structural differences between the two synthesized phases.

It should be noted that the diffractograms indicate the presence of a small peak at 12.64° corresponding to PbI_2 phase. This peak has been often identified in thin film X-ray diffraction and is an indicator of a slight decomposition of the samples. These results suggest that the presence of the impurity phase PbI_2 is due to the solution interaction $FAPbBr_3/FAPbI_3$ that leaves a small amount of $FAPbI_3$ (150°C) unreacted, thus leaving a corresponding amount to PbI_2 formation. However, as one can notice in Fig. 2b, the formation of PbI_2 was negligible and the perovskite peaks were dominant. The additional peak observed previously at 12.6° disappears with decreasing of iodide contents. The disappears of PbI_2 phase in the diagrams proves that our mixed perovskite becomes more stable with the addition of bromide.

The high crystallinity of the synthesized FAPbI3, FAPbBr3 and FAPbBr3-xIxwas highlighted by the sharp diffraction peaks. This finding is fairly coherent with the literature [41].

The diffraction angle shift indicated that the two ions Br and I are both inserted in the same lattice, at the meanwhile, the shift of the peak maximum toward lower angle for (x=0-3) indicates an increase in lattice parameter. The changes in the lattice parameter are probably due to the incorporation of the larger I anion instead of the smaller Br anion (the ionic radii of Br and I are 1.96 Å and 2.20 Å, respectively) [42, 43].

The lattice parameters of $FAPbBr_{3-x}I_x$ shown in Table 1 are extracted from the (001) peak. The contraction of the lattice with increasing iodide contents (Fig. 2a) confirms the substitution of the bromide anion by iodide. The calculated lattice parameters of $FAPbBr_3$ and $FAPbI_3$ are a = 5.993 Å and a = 6.352 Å respectively which is in good agreement with the previously reported phase of $FAPbI_3$ and $FAPbBr_3$ [27, 44]. In addition, for different iodide contents the $FAPbBr_{3-x}I_x$ keeps the same cubic phase. The lattice parameter of $FAPbBr_{3-x}I_x$ ($0 \leq x \geq 3$), which exhibits a linear relationship with the [Br/I] contents in each region, increases with the increase of iodide contents. Therefore, the linear trend indicates the formation of the $FAPbBr_{3-x}I_x$ with a change of the lattice parameter rather than the phase of $FAPbI_3$ and

$FAPbBr_3$. This illustrates that it is not trivial to determine the (Br, I) contents from lattice parameters deduced from XRD measurements.

The amount of Br and I in thin films were determined by elemental analysis using EDX. The space group (Pm-3m for both materials) and unit cell parameters (a = 5.9944 Å for $FAPbBr_3$ and a = 6.3573 Å for α-$FAPbI_3$) measured by XRD were found to be consistent with those from previous reports [39, 45].

Table 1: Lattice parameter (a) of $FAPbBr_{3-x}I_x$ (x= 0-3) film and crystallite size for the (001) diffraction planes.

$FAPbBr_{3-X}I_X$	0	0.4	0.8	1.2	1.6	2	3
a /Å	5.993	6.037	6.089	6.112	6.206	6.247	6.352
Crystallite size (Å)	1020	810	620	450	410	320	280

Table 1 also displays the crystallite size obtained from the Scherrer formula [46] applied to the (001) peak. As can be seen the crystallite size decreases as Br concentration decreases and ranges from 1020 Å to 280 Å for $FAPbBr_3$ and $FAPbI_3$, respectively.

Fig 3 shows the evolution of the interplanar spacing as a function of Br/I ratio. This distance is proportional to the amount of bromide. In other words, it increases with the increase f iodide quantity. This behavior can be explained by the ionic radius of both elements. In fact, the ionic radius of Br and I are 1.96 Å and 2.20 Å, respectively. We can clearly see that the ionic radius of I is greater than Br and as a result influences the interplanar distance.

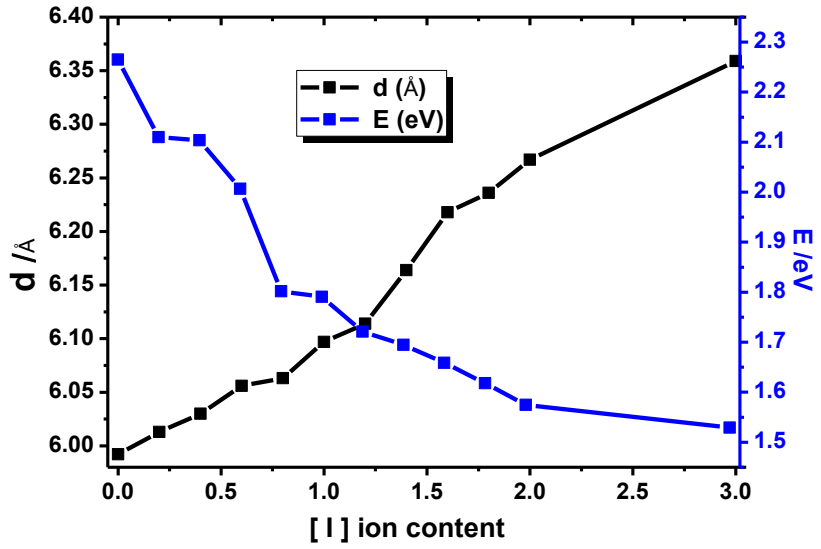

Fig. 3 Interplanar spacing (*d*) and optical gap (*Eg*) as a function of [Br / I] ratio.

2.2. SEM and EDX analyses

Fig. 4 shows the scanning electron micrographs of FAPbBr1-xIx thin films deposited onto ITO-glass substrate with different [Br]/[I] ratios. As can be seen from this figure, the effect of [Br]/[I] ratios is visible on the aspect of the surface film. All micro-structures consist of grains with certain porosity. As illustrated in fig.4a, films prepared with only Br element show rough organization with some holes on the surface. For $0 \leq x \leq 0.8$, the micrographs of thin films reveal non-uniform grain sizes and non-homogeneous surface with mixture of smaller and larger clusters.

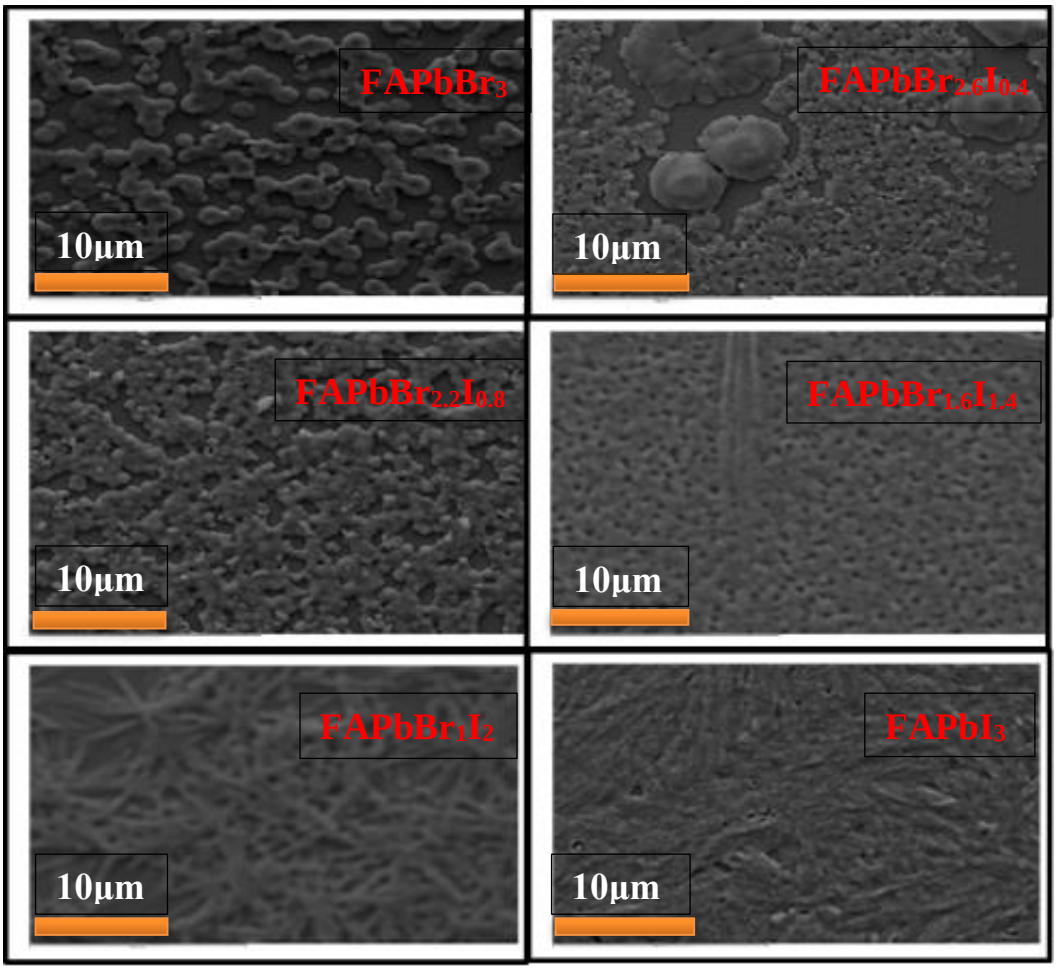

Fig.4 FESEM images of $FAPbBr_{3-x}I_x$ thin films prepared on glass/ITO substrates.

FESEM images show the dependence of the grain size on the iodide contents. The obtained films with different iodide contents have a different shape, morphology and size. Indeed, as the composition x increases, the aggregation of gains increased [47, 48]. This effect can be related to the electron beam while the films are observed by SEM. This behavior could indicate fragile grain boundaries, which potentially lead to a problem in charge carrier transport through the grain boundaries. This result was also obtained by Anand et al. [49], who have synthesized $FAPbBr_3$ by spin coating technique. When the percentage of iodide increases (Fig. 4 for x=0.8,

1.4 and 2), we notice a reduction of clusters size giving a densely packed and nearly homogeneous surface consists of small grains. This reduction reinforces the densification of the $FAPbBr_{1-x}I_x$ films and reduces the leakage current due to grain boundaries. The same micrograph was obtained by Vanessa et al., who have synthesized pure $FaPbI_3$ [50].

It is worth to highlight that the crystallite sizes obtained by the Scherrer equation are smaller than those observed from SEM. This indicates that the $FAPbBr_{3-x}I_x$ grains as observed by SEM images are composed of several crystallites.

Table 2: EDX data of the variation of the atomic percentage between the Iodine, Lead and bromide for $FAPbBr_{3-x}I_x$ thin films (x= 0 - 3).

	Atomic % Pb	Atomic % Br	Atomic % I
$FAPbBr_3$	23.64	76.36	0
$FAPbBr_{2.6}I_{0.4}$	22.96	64.74	12.30
$FAPbBr_{2.2}I_{0.8}$	21.96	55.40	22.64
$FAPbBr_2I_1$	22.03	51.41	26.56
$FAPbBr_{1.6}I_{1.4}$	20.81	42.67	36.52
$FAPbBr_{1.2}I_{1.8}$	23.11	31.36	45.54
$FAPbBr_1I_2$	22.20	28.73	49.07
$FAPbI_3$	23.25	0	76.75

Table 2 presents the EDX results for all synthesized $FAPbBr_{3-x}I_x$samples. These results indicate that FA, Pb, Br and I are homogeneously distributed in the perovskite crystal, suggesting that Pb and Br/I are uniformly incorporated in the $FAPbI_3$, $FAPbBr_3$ and $FAPbBr_{3-x}I_x$ films in the grain perovskite rather than in separate chemical phases. The results of EDX

analysis indicate that all films present a deficit of Pb. The measured ratio for Pb:I, Pb:Br and Pb:I+Br is in the range of 21-24%, which is slightly lower than the expected theoretical value (25%).

2.3. UV-vis analyses

The differences in the structural and morphological features have a dramatic influence on the optical properties of the prepared materials. In Fig 5, the absorbance for $FAPbBr_{3-x}I_x$ (x=0-3) thin films is shown.

It is important to notice that for absorption measurements we used an integrating sphere to collect both specular and diffuse transmittance in order to remove the effect of light scattering originating from refraction and reflection phenomena inside the perovskite crystals. Comparing to both compound presented in figure 5a, we can note that the FAPbI3 present a wider range absorbance than $FAPbBr_3$. In fact, the absorption in the visible range is attributed to the difference between the conduction and the valence band, which indicates that the substitution of Br by I leads to a decrease of band gap energy. The values of *Eg* as a function of anions' composition are summarized in Table 3.

These materials exhibit optical bandgaps that match with the different colors of the films. For the $FAPbX_3$ (X=I, Br), the data at wavelengths below 841 nm for X = I and 558 nm for X = Br have been omitted due to dispersion and diffusion effects. A comparison between Fig.

5a and Fig. 5b reveals that the absorption properties of perovskite films differ significantly from the precursor (Br-Pb-I) confirming further the transformation into perovskite structure Br/I. Hence, the presence of a single emission peak close to the absorption edge is a proof of a single phase of the perovskite structure.

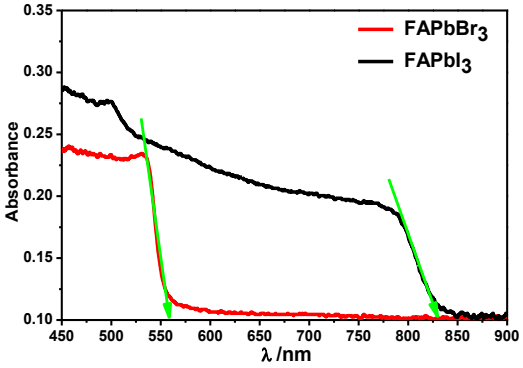

Fig. 5a Absorbance of $FAPbI_3$ and $FAPbBr_3$ films deposited on ITO substrates.

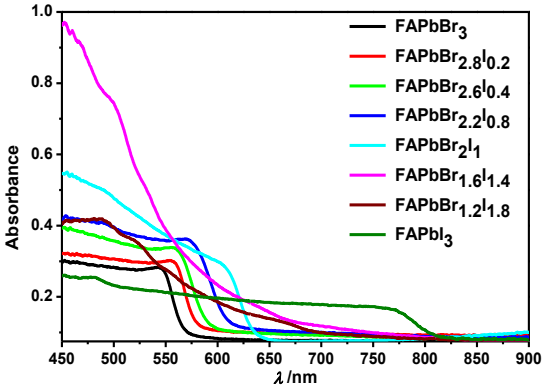

Fig. 5b Absorbance spectra of $FAPbBr_{3-x}I_3$ (x = 0-3) films deposited on ITO substrates.

These results confirm that the observed emission arises from charge carrier recombination within the band structure of mixed halide perovskites films. It is interesting to note that the difference absorption spectra of all mixed halide perovskites films (Fig. 5b) exhibit similar spectral prints of induced absorption and bleaching of the absorption band. The only difference is the position of the maximum, which shifts to red as the iodide contents increases. The position of the bleaching maximum agrees well with the absorption edge for the corresponding perovskite film. This spectral feature, in turn, indicates a common semiconducting behavior of mixed

halide perovskites despite the difference in the halide composition. For formamidinium lead bromide iodide mixed halide perovskites $FAPbBr_{3-x}I_x$, the absorption of photons with energy similar to that of the bandgap, $Eg \cong hv$, leads to an optical transition producing an electron in the conduction band and a hole in the valence band (exciton) in order to explore the range of bandgap tunability of the formamidinium lead trihalide system [19]. Indeed, strong size confinement effects can be observed in nanocrystalline systems when their crystal size becomes smaller than the exciton Bohr diameter.

According to the optical absorption measurements shown in Fig. 5a, a decrease of the bandgap energy by increasing the ionic radius of the anion in the $FAPbX_3$ systems can be observed. For X = I, the bandgap has a value of 1.48 eV, which is consistent with the data reported in the literature [19]. These authors also found that Pb-based phases have optical bandgaps that are independent of the preparation method. By comparing to the values obtained from Fig 5c, the extrapolation gave an *Eg* of 1.48 eV for $FAPbI_3$ and an *Eg* of 2.3 eV for $FAPbBr_3$, which are confirmed by the literature [19, 51]. The shift of the bandgaps might be due to the presence of PbI_2 impurity phase in the prepared samples for (x=1.2-1.8) proved by XRD. The absorption spectra in Fig. 5b show that the bandgap increases with bromide fraction from about 1.48 to 2.22 eV. These results are in good agreement with theory, which predicts that the larger the ion size (Br) the smaller the

Eg is. The fact that the mixture shows peaks from both samples ($FAPbBr_3$, $FAPbI_3$ and $FAPbBr_{3-x}I_x$) indicates that a mixture of the two samples was formed. In addition, the *Eg* of the mixture is between the bandgap energies of $FAPbBr_3$ and $FAPbI_3$ which is a further support claiming that a new phase has been synthesized.

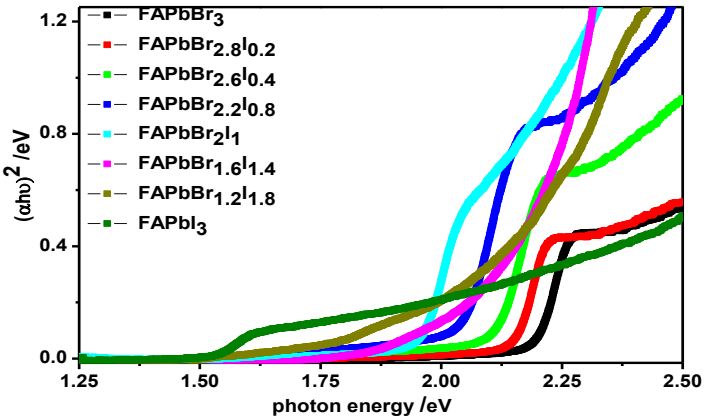

Fig. 5c Estimation of the optical band gap (c) of $FAPbBr_{3-x}I_3$ (x = 0-3) films on ITO substrates.

The systematic shift in the position of the absorption edge of $FAPbBr_{3-x}I_x$ thin films to lower wavelengths, observed as the concentration of Br decreased, is illustrated in Table 3. As the iodide contents decreases, the absorbance edge shifts to short wavelength values, indicating the increase of the bandgap energy of the prepared perovskite thin films. The onset bandgap of mixed (Br, I) perovskite thin films are located in intermediate values between 1.48 eV ($FAPbI_3$) and 2.3 eV ($FAPbBr_3$) meaning that the bandgap can be tuned by varying the composition of the ratio Br/I.

2.4. Luminescence properties

Organometal halide perovskites also emit strong room temperature photoluminescence (PL) that arises from excitons (radiative recombination of charge carriers) in the inorganic sheets [52]. PL measurements of films prepared by the one-step deposition method were complicated by the appearance of the yellow δ-phase of the formamidinium iodide, which optically manifests low only the prepared $FAPbI_3$thin films. The absence of the α-phase explains the blue-shifted emission in $FAPbI_3$ prepared by deposition method with different temperature annealing (Fig. 6a). These results are confirmed by the evolution of the wavelength for $FAPbI_3$from λ = 791 nm when T=140 °C to λ= 810 nm when T= 150°C, and thus it involves the passage to the most stable phase the α—δ, which is confirmed by the results of XRD [53].

We compare the PL results shown in Fig. 6b of $FAPbBr_{3-x}I_x$ formed with a different fraction of Br/I. Intensities are normalized to clarify the shift of the emission peaks. A systematic shift in the position of the peaks to lower wavelengths is observed as the concentration of bromide increases. This indicates that the recombination centers come probably from the presence of the bromide and iodide in the perovskite lattice, which is in good agreement with the XRD analyses and absorbance spectra. These observations are consistent with the literature [24], suggesting a clean bandgap and one photo-

active species from which emission arises in the Br/I lead perovskites films and indicating that the transition between perovskites occurs via mixed halide.

Table 3: Changes in the peak positions (001) and wavelength in PL and absorption with the variation of Br and I.

	(001)	λ_{Abs}/nm	E_{Abs}/eV	λ_{PL}/nm	E_{PL}/eV
$FAPbBr_3$	14.78	558.6	2.22	547.3	2.26
$FAPbBr_{2.6}I_{0.4}$	14.68	604.3	2.05	589.1	2.10
$FAPbBr_{2.2}I_{0.8}$	14.60	632.7	1.96	687.9	1.80
$FAPbBr_2I_1$	14.52	664.8	1.86	692.4	1.79
$FAPbBr_{1.6}I_{1.4}$	14.36	715.6	1.73	731.4	1.69
$FAPbBr_{1.2}I_{1.8}$	14.19	770.1	1.61	766.1	1.62
$FAPbBr_1I_2$	14.12	792.2	1.56	787.1	1.57
$FAPbI_3$	13.92	840.3	1.47	810.5	1.53

The PL spectra of the films displayed in Fig. 6b show single transitions with a monotonic shift in peak position with increasing iodide content from pure tri-bromide perovskite (2.26 eV) to pure triiodide perovskite (1.53 eV). This finding supports our observation of a clean bandgap in these films. However, mixing the halide component with the perovskite offers the finest tuning of the optical properties of the perovskite film. Here, the mixed organic lead iodide/bromide system has recently gained strong interest for application in perovskite solar cells [19, 34]. By changing the ratio between bromide and iodide (at the X site anion), the bandgap can be tailored between 1.53eV ($FAPbI_3$) and 2.26 eV ($FAPbBr_3$) in agreement with previous reports [54], which results in the coverage of much of the visible spectrum and paves the way for the development of tandem solar cell [31]. The analysis of figure

6b indicates that the substitution of Br by I leads to a red shift in the spectrum. Also, we can see that the photoluminescence spectra contain several peaks with low intensity, which means that, apart from inter band transitions, other radiative transitions between the valence and/or conduction bands and some energy levels located inside the bandgap are involved. The component of PL spectra with the highest energy corresponds to transitions from the conduction band to the valence band and the lower energy components of the PL spectra involve energy levels inside the bandgap, which is in agreement with the sub bandgap absorption mentioned before.

The high intensity of PL emission suggests that most decay transitions are radiative and nonradiative decay is negligible. Since the radiative recombination dominates, one can deduce that most energy levels within the bandgap correspond to shallow levels and electron-hole pairs formed during the optical excitation recombining radiatively emitting photons. A number of deep levels inside the bandgap is very low and as a result, both pure and mixed perovskites exhibit high luminescent efficiency. Theoretical calculations show that the red shift upon moving from Br^- to I^- derives from the associated decrease of the electronegativity of the halogen atom [35,55]. Exchanging Br^- with I^- changes the nature of the halide frontier orbital contribution to the valence band, which reduces the bandgap energy [56, 57]. The observed PL peak positions are consistent with the absorption onsets

seen in the absorbance spectra of the examined $FAPbBr_{3-x}I_x$ films, confirming that the PL arises primarily from band-edge emission rather than from minority phases or trap states.

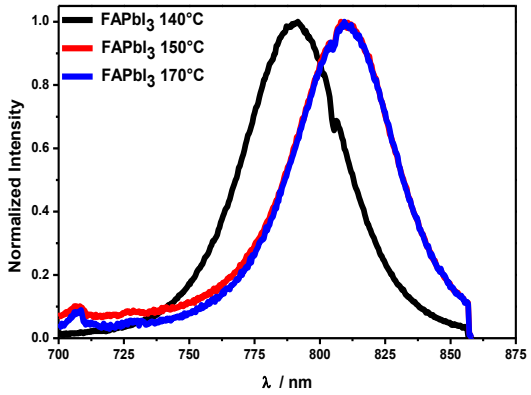

Fig. 6a Normalized PL spectra of $FAPbI_3$ thin films at different annealing temperatures.

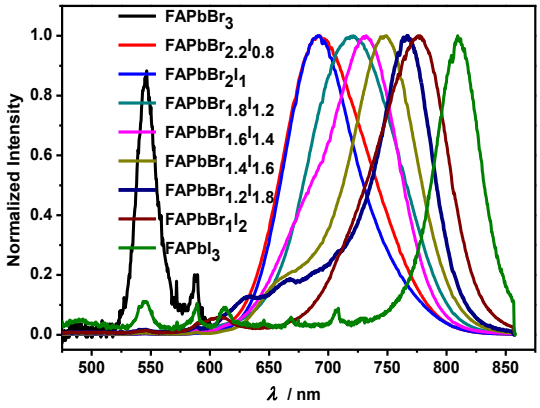

Fig. 6b Normalized PL spectra at room temperature for $FAPbBr_{3-x}I_x$ (x =0-3) thin films.

Table 3 displays the position of the most intense PL peak and the related wavelength at room temperature for different $FAPbBr_{3-x}I_x$ (x= 0-3) perovskite thin films. For these samples, the wavelength position of the maximum of PL emission is shifted to lower wavelengths when compared with the onset of the absorption edge.

3. Conclusion

The organic–inorganic perovskites $FAPbBr_{3-x}I_x$ were prepared by mixing $FAPbBr_3$ and $FAPbI_3$ in the desired proportions (x=0-3) and deposited as thin films onto ITO substrates by spin coating in only one-step. Our results show that changing the molar ratio Br/I in the precursor solution

has a significant effect on the morphology, optical absorption and PL properties of $FAPbBr_{3-x}I_x$.

All the synthesized $FAPbBr_{3-x}I_x$ (x=0-3) perovskites reported in this paper crystallized in the same cubic phase (space group Pm-3m) independently of the x value. The shift of diffractions peaks towards low angles is directly related to the increase of the iodide contents.

Absorbance measurements show that $FAPbBr_{3-x}I_x$ perovskite films exhibit a very high absorbance for a high concentration of iodide. It was found that the onset of the absorption edge for $FAPbBr_{3-x}I_x$ thin films reaches intermediate values ranging from 1.48 eV ($FAPbI_3$) to 2.3 eV ($FAPbBr_3$). Room temperature PL emission can be tuned from 548 nm for $FAPbBr_3$ to 810 nm for$FAPbI_3$ by varying the Br/I ratio. Perovskites with high iodide contents as well as pure bromide perovskites have a clean PL-spectrum with emissions from a single region centered at the optical bandgap energy. These PL emissions appear to be stable over time. Finally, the results obtained confirmed that mixed $FAPbBr_{3-x}I_x$ perovskites are promising materials for applications in light emitting and photovoltaic devices.

4. Experimental

4.1. Synthesis of Formamidinium Iodide and Formamidinium Bromide (FAI and FABr)

To synthesize mixed halides $FAPbBr_{3-x}I_x$ perovskites, both formamidinium iodide ($HC(NH_2)_2I$ or FAI) and formamidinium bromide ($HC(NH_2)_2Br$ or FABr) were first prepared by directly mixing formamidine acetate with hydroiodic acid (HI) or hydrobromic acid (HBr) at 0 °C.

$CH(NH_2)_2I$ or $CH(NH_2)_2Br$ was synthesized by slowly dissolving formamidinium acetate powder in HI (57 wt% in water, from Sigma-Aldrich) or HBr (48 wt % in water, from Sigma Aldrich) in a molar ratio of 1:1, the mixture was stirred for 30 min in a round-bottom flask, which was kept in an ice bath (0 ºC). The solvent was evaporated using a rotary evaporator and the solid was re-crystallized in ethanol two times, and then dried again. The product obtained was collected by filtration after having been washed thoroughly using diethyl ether until a white crystalline solid was obtained. The solids were finally dried under vacuum for one night before use.

4.2. Synthesis of Formamidinium Lead Iodide powders

$FAPbI_3$ perovskite powder was synthesized by mixing 0.08 mol hydroiodic acid(HI) (57 wt. % in H_2O, distilled, stabilized, 99.95% from Sigma Aldrich) and 3.1 mL hypophosphorous acid (H_3PO_2). The mixture

was stirred for 30 min in a 250 mL round-bottom flask, which was kept in an ice bath (0 ºC).Then 0.075 mol of formamidinium acetate powder previously dissolved in 20 mL of distilled water was added drop-wise. Subsequently, this mixture was heated up to 100 ºC for 30 minutes and then 0.008 mol of lead (II) acetate trihydrate previously dissolved in 30 mL of distilled water maintained at 60 °C, was added drop-wise under vigorous stirring. The solution was kept at 100 °C for 1 hour with stirring and reflux. After this process, a precipitate of black crystalline powder takes place. The remaining solution was then left to cool until 50 ºC and was then filtered. The crystalline powders were washed several times with absolute ethanol, diethyl ether and then dried under vacuum for 15 min. Finally, the powder was annealed at different temperatures (140 °C and 180 °C) for 2 hours.

By elemental analysis, it was found that the weight ratio of C: N: H: (I:Br) in the as-prepared FAI and FABr was 7.30:16.46:2.83:73.41 and 9.48:21.81:3.98:64.82, respectively, which is in very good agreement with theoretical atomic ratio of 1:2:5:1(C: N: H:(I,Br))which are presented in Table 4. FAI and FABr were very pure with no presence of any other impurity, as verified by XRD. It was found that the mixture of FAI, FABr, PbI_2 and $PbBr_2$ with molar ratios of 1:1 was soluble in DMF.

Table 4: The theoretical and experimental results of the atomic ratio of FAI and FABr

Elements	C	N	H	I	Br
FAI	1	2	5	1	0
Theoretical atomic ratio	6.98	16.29	2.91	73.82	0
Experimental Atomic ratio	7.30	16.46	2.83	73.41	0.00
FABr	1	2	5	0	1
Theoretical atomic ratio	9.61	22.42	4.00	0.00	63.97
Experimental atomic ratio	9.48	21.81	3.98	0.00	64.82

4.3. Synthesis of thin film perovskites $FAPbBr_{3-x}I_x$ (x=0-3)

$FAPbBr_{3-x}I_x$ (x=0-3) thin films were deposited by a single-step spin-coating method. The $FAPbBr_{3-x}I_x$ precursor solutions were prepared by dissolving FAI, FABr, PbI_2 and $PbBr_2$ with equimolar mixture molar ratios1:1 in N, N-dimethyl-formamide (DMF) solvent at 40% wt. The precursor solutions were stirred at 60°C for 30 min and then deposited on ITO-coated glass substrates by spin coating at 3500 rpm for 11s. Then, a drop of toluene was added and finally, dried at 5000 rpm for 30s. Some of the deposited layers were kept in dry air at room temperature and others were annealed in vacuum at 140 and 150 °C for 30 min.

4.4. Characterization

The X-ray diffraction (XRD) patterns of the prepared films were measured using a RIGAKU Ultima IV diffractometer equipped with $Cu_{K\alpha}$ radiation (λ=1.5406 Å). The morphology of the films was observed using a

field-emission scanning electron microscope (MIRA3 LMU, Tescan). The elemental analysis (C, H, N and S) of the perovskite was performed using a FISONS EA_1108 CHN analyzer, with a high-resolution scanning electron microscope (FE-SEM) at an acceleration voltage of 10 kV. Photoluminescence (PL) spectra were recorded at room temperature using a He-closed cryostat. The PL excitation source was a He-Cd laser emitting at 325 nm. Photoluminescence data were recorded by a Si-based CCD detector Hamamatsu. Optical measurements were performed at room temperature using a spectrometer Ocean Optics HR4000 equipped with a Si-CCD detector. An integrating sphere was used to collect both direct and diffuse transmittance.

Acknowledgements: This work was supported by Ministerio de Economía y Competitividad (ENE2016-77798-C4-2-R) and Generalitat valenciana (Prometeus 2014/044).

References

1. Kojima A, Teshima A, Shirai Y, Miyasaka T (2009) J Am Chem Soc 131:6050

2. Etgar L, Gao P, Xue Z, Peng Q, Chandiran AK, Liu B, Nazeeruddin MK, Gratzel M (2012) J Am Chem Soc 134:17396

3. Zhang K, Eperon GE, Snaith HJ (2016) Nat Energy 1:16048

4. Zuo C, Bolink HJ, Han H, Huang J, Cahen D, Ding L (2016) Adv Sci 3:1500324

5. Wang YK, Yuan ZC, Shi GZ, Li YX, Li Q, Hui F, Sun BQ, Jiang ZQ, Liao LS (2016) Adv Funct Mater 26:1375

6. Yang WS, Noh JH, Jeon NJ, Kim YC, Ryu S, Seo J, Seok SII (2015) Science 348:1234

7. Zhang F, Zhong H, Chen C, Wu XG, Hu X, Huang H, Han J, Zou B, Dong Y (2015) ACS Nano 9:4533

8.Braly IL, Hillhouse HW (2016) J Phys Chem C 120:893

9. Hu M, Bi C, Yuan Y, Bai Y, Huang J (2016) Adv Sci 3:1500301

10. Jeon NJ, Noh JH, Yang WS, Kim YC, Ryu S, Seo J, Seok S (2015) Nature 517:476

11. Im J, Jang I, Pellet N, Grätzel M, Park N (2014) Nat Nanotechnol 9:927

12. Liu J, Lu S, Zhu L, Li X, Choy WCH (2016) Nanoscale 8:3638

13. Jung HS, Park NG (2015) Small 11:10

14. Yang Z, Chueh CC, Liang PW, Crump M, Lin F, Zhu Z, Jen AKY (2016) Nano Energy 22:328

15. Zhou Y, Yang M, Wu W, Vasiliev AL, Zhu K and Padture NP (2015) J Mater Chem A3:8178

16. Shao S, Chen Z, Fang HH, Brink GH, Bartesaghi D, Adjokatse S,

Koster LJA, Kooi BJ, Facchetti A, Loi MA (2016) J Mater Chem A 4:2419

17. McMeekin DA, Sadoughi G, Rehman W, Eperon GE, Saliba M, Hörantner MT, Haghighirad A, Sakai N, Korte L, Rech B, Johnston MB, Herz LM, Snaith HJ (2016) Science 351:151

18. Koh TM, Fu K, Fang Y, Chen S, Sum TC, Mathews N, Mhaisalkar SG, Boix PP and Baikie T (2014) J Phys Chem C118:16458

19. Jacobsson TJ, Baena JPC, Pazoki M, Saliba M, Schenk K, Gratzel M, Hagfeldt A (2016) Energ Environ Sci 9:1706

20. Kim YC, Jeon NJ, Noh JH, Yang WS, Seo J, Yun JS, Ho-Baillie A, Huang S, Green MA, Seidel J, Ahn TK, Il Seok S (2016) Adv Energ Mater 6:457

21.Wozny S, Yang M, Nardes AM, Mercado CC, Ferrere S, Reese MO, Zhou W and Zhu K (2015) Chem Mater 27:4814

22. Lv S, Pang S, Zhou Y, Padture NP, Hu H, Wang L, Zhou X, Zhu H, Zhang L, Huang C and Cui G (2014) Phys Chem Chem Phys 16:19206

23. Han Q, Bae SH, Sun P, Hsieh YT, Yang Y, Rim YS, Zhao H, Chen Q, Shi W, Li G and Yang Y (2016) Adv Mater 28:2253

24. Aharon S, Dymshits A, Rotem A and Etgar L (2015) J Mater Chem A 3:9171

25. Zhu K, Miyasaka T, Kim JY and Seró IM (2015) J Phys Chem Lett 6:2315

26. Brivio F, Caetano C, Walsh A (2016) J Phys Chem Lett 7:1083

27. Bai S, Yuan Z, Gao F (2016) J Mater Chem C 4:3898

28. Binek A, Hanusch FC, Docampo P, Bein T (2015) J Phys Chem Lett 6:1249

29. Wang Z, Zhou Y, Pang S, Xiao Z, Zhang J, Chai W, Xu H, Liu Z, Padture NP and Cui G (2015) Chem Mater 27:7149

30. Zhou Y, You L, Wang S, Ku Z, Fan H, Schmidt D, Rusydi A, Chang L, Wang L, Ren P, Chen L, Yuan G, Chen L, Wang J (2016) Nat Commun 7:11193

31. Yi C, Luo J, Meloni S, Boziki A, Ashari-Astani N, Gratzel C, Zakeeruddin SM, Rothlisberger U, Gratzel M (2016) Energy Environ Sci 9:656

32. Vega E, Mollar M and Marí B (2015) Phys Status Solid C 1-5

33. Atourki L, Vega E, Marí B, Mollar M, Ahsaine HA, Bouabid K, Ihlal A (2016) Appl Surf Sc 371:112

34. Yoon SJ, Draguta S, Manser JS, Sharia O, Schneider WF, Kuno M, Kamat PV (2016) ACS Energy Lett 1:290

35. Rehman W, Milot RL, Eperon GE, Wehrenfennig C, Boland JL, Snaith HJ, Johnston MB, and Herz LM (2015) Adv Mater 48:7938

36. Price M, Butkus J, Jellicoe T, Sadhanala A, Briane A, Halpert J, Broch K, Hodgkiss J, Friend R, Deschler F (2015) Nat Commun 6:8420

37. Zhu H, Miyata K, Fu Y, Wang J, Joshi P, Niesner D, Williams KW, Jin S, Zhu XY (2016) Science 353:1409

38. Saliba M, Matsui T, Seo JY, Domanski K, Correa-Baena JP, Mohammad KN, Zakeeruddin SM, Tress W, Abate A, Hagfeldt A, Grätzel M (2016) Energy Environ Sci 9:1989

39. HanuschFC, Wiesenmayer E, Mankel E, Binek A, Angloher P, Fraunhofer C, Giesbrecht N, Feckl JM, Jaegermann W, Johrendt D, Bein T, Docampo P (2014) J Phys Chem Lett 5:2791

40. Aygüler MF, Weber MD, Puscher BMD, Medina DD, Docampo P, Costa RD (2015) J Phys Chem C 119:12047

41. Jeon NJ, Noh JH, Kim YC, Yang WS, Ryu S and Seok SI (2014) Nat Mater 13:897

42. Lee JW, Kim DH, Kim HS, Seo SW, Cho SM, Park NG (2015) Adv Energy Mater 5:1501310

43. Yuan DX, Gorka A, Xu MF, Wang ZK, Liao LS (2015) Phys Chem Chem Phys 17:19745

44. Weller MT, Weber OJ, Henry PF, Di Pumpo AM, Hansen TC (2015) Chem Commun 51:4180

45. Weller MT, Weber OJ, Frost JM, Walsh A (2015) J Phys Chem Lett 6:3209

46. Scherrer P (1918) Goettinger Nachrichten Math Phys 2:98

47. Yang Z, Chueh CC, Liang PW, Crump M, Lin F, Zhu Z, Jen AKY (2016) Nano Energy 22:328

48. Kyung TC, Sanghyun P, Giulia G, Cristina RC, Peng G, Yonghui L, Mohammad KN (2017) Energy Environ Sci 10:627

49. Anand SS, Sumanshu A, Neha M, Pradeep N, Maikel VH, Shaibal KS (2015) Adv Mater Interfaces 7:1601143

50. Vanessa LP, Benjia D, Douglas GVC, Talysa RKS, Frank SB, Sean ES, Ahmed MI, Maikel FAM, Michael FT (2017) Nat Comm 8:14075

51. Tsunekawa S, Fukuda T, Kasuya A. (2000) J. Appl. Phys. 87:1318

52. Papavassiliou GC and Koutselas IB (1995) Synth Met 71:1713

53. Koh T, Fu K, Fang Y, Chen S, Sum T, Mathews N, Mhaisalkar S, Boix P and Baikie T (2014) J Phys Chem C 118:16458

54.Jacobsson TJ, Tress W, Correa-Baena JP, Edvinsson T, Hagfeldt A (2016) J PhysChem C 120:11382

55. Gao P, Grätzel M, Nazeeruddin MK (2014) Energy Environ Sci 7:2448

56. Walsh A (2015) J Phys Chem C 119:5755

57.Mosconi E, Amat A, Nazeeruddin MK, Grätzel M, Angelis FD (2015) J Phys Chem C 117:13902